

Article

Hydrocracking of Light Diesel Oil over Catalysts with Industrially Modified Y Zeolites

Mengna Zhang ^{1,†}, Bo Qin ^{2,†}, Weimin Zhang ¹, Jiajun Zheng ¹, Jinghong Ma ^{1,*} , Yanze Du ² and Ruifeng Li ¹

¹ Institute of Special Chemicals, College of Chemistry and Chemical Engineering, Taiyuan University of Technology, Taiyuan 030024, China; zhangmengna0541@link.tyut.edu.cn (M.Z.); zhangweimin0071@link.tyut.edu.cn (W.Z.); zhengjiajun@tyut.edu.cn (J.Z.); rfli@tyut.edu.cn (R.L.)

² Dalian Research Institute of Petroleum & Petrochemicals, SINOPEC, Dalian 116045, China; qinbo.fshy@sinopec.com (B.Q.); duyanze.fshy@sinopec.com (Y.D.)

* Correspondence: majinghong@tyut.edu.cn; Tel./Fax: +86-351-6010121

† These authors contributed equally to this work.

Received: 25 June 2020; Accepted: 15 July 2020; Published: 22 July 2020



Abstract: Three industrially modified Y zeolites with a hierarchical structure were characterized by XRD, N₂ adsorption–desorption, SEM, TEM, ²⁷Al-/²⁹Si-NMR, in situ pyridine-FTIR, and NH₃-TPD techniques. The industrial hydrocracking catalyst of light diesel oil was prepared by kneading and extruding the mixture of 10 wt.% industrially modified zeolite, commercial alumina, nickel nitrate, and molybdenum oxide. The small amount of hierarchical Y zeolite in the hydrocracking catalyst plays a key role, resulting in selective hydrogenation of naphthalene and further ring-opening activity. The mesoporous structure of the zeolites provided an effective interface and improved the accessibility of acid sites to bulky reactants.

Keywords: Y zeolite; hydrocracking; light diesel oil; micro-mesoporosity; acidity

1. Introduction

Hydrocracking of heavy oils is a very important process for petroleum conversion, in which high-molecular-weight hydrocarbons are converted to low-molecular-weight hydrocarbons [1]. Most of the conventional hydrocracking catalysts are bifunctional catalysts, whose functions involve hydrogenation–dehydrogenation by metal components and acid cracking over zeolites [2]. The hydrogenation–dehydrogenation processes over the metallic component realizes the conversion of aromatics to naphthenics, and the acid sites, usually afforded by the zeolite component, actually trigger the cracking roles of C–C bonds of naphthenes and partial lateral chains [3]. In the available literature, zeolites Y, ZSM-5, and β , and even some ordered mesoporous materials, such as SBA-15 and MCM-48, were frequently reported to be used as the cracking components to yield the acid sites of the hydrocracking catalysts. Metals of Mo, Ni, W, Pd, and Pt were often reported to serve the hydrogenation–dehydrogenation purpose of the bifunctional catalysts [4–9]. Moreover, in these reports, Y zeolite, with its high hydrothermal stability, suitable microporous size, good ions exchange capacity, and excellent shape selectivity, has been frequently used as the cracking component and applied widely in the hydrocracking processing [10].

Zeolite Y with the faujasite (FAU) structure is a commonly used acid catalyst in fluid catalytic cracking (FCC), hydrocracking, isomerization, or esterification [11–14]. The zeolite has a considerable large supercage, with a diameter of 1.3 nm, connected to the tetrahedron with four adjoining cages, each with a diameter of 0.74 nm [15]. However, for bulky reactant molecules, on the one hand, a remarkable diffusion limitation occurs in Y zeolite because of its bigger kinetic diameters of the reactants when

moving in the micropores' channels; on the other hand, the cages in the pore system easily capture the guest molecules (either the reactants or the products, even the intermediate products) to form traps to obstruct the products' rapid escaping from the channels by shielding the purging of the carrier gas flows. In consequence, it often leads to a secondary cracking [2,16]. Moreover, Y zeolite may suffer from a fast passivation caused by the deposit of the formation coke on the active sites, which may not only cause severe diffusion limitation as reflected in weakening mass and heat transfer, but also lead to the dramatic decrease of the acid sites in the zeolitic micropores [17]. In order to overcome these disadvantages, the modification via introducing meso-or/and macropores into zeolite crystals has been widely reported. For zeolite Y, the modification was usually represented by templating and non-templating methods. The templating strategy involves using soft or hard templates as the pore-forming agent for fabricating a hierarchical pores system in the as-synthesized Y zeolite crystals during the synthesis process. When the templates are removed, meso- or/and macro-pores were left in the zeolite crystals where the templates used to be located [18–20]. Martínez and his co-workers introduced mesopores into zeolite Y crystals by using a surfactant as a template. The as-made mesopore-structured Y zeolite was reported to have superb hydrothermal stability, while keeping its strong acid properties. Due to the introduced mesopores, the mesoporous zeolite as FCC catalyst displayed a modified diffusion property and an improved selectivity in aimed products [18]. However, the high cost of templates may be a concern for large-scale application, and the removal of templates by calcination may also bring potentially environmentally unfriendly behavior [21]. The non-templating method is represented by a post-treatment which may include steaming, acid etching, alkali etching, or complicated treatments combining steaming, acid etching, and/or alkali etching on the zeolite crystals, so as to cause desilicication or dealumination from the zeolite crystals and thus introduce mesopores into zeolite Y [22–25]. Yan et al. investigated the dealumination of USY zeolites by nitric acid and oxalic acid treatment. The result suggests that both the above acids are effective in removing the framework and non-framework Al [25]. In these studies, either the extent of created mesopores or the size of introduced secondary pores in the zeolites has a great effect on catalytic activity and selectivity [26]. The recrystallization of the ultra-stable zeolite Y produced micro-mesoporous structure and significantly increased the intracrystalline mesoporosity in zeolite, and the concentration of strong Brønsted acid sites in the NiMo/USY-Al₂O₃ hydrocracking catalysts was adjusted by the recrystallization degree of the zeolite [27]. The catalyst composed of recrystallized zeolite showed significantly higher activity in hexadecane hydrocracking than the catalyst obtained by using parent zeolite, due to the improved accessibility of its active sites. The available metal active sites and acid sites have improved the hydrogenation activity and cracking selectivity of the catalyst; the metal–acid balance of the catalyst shifted toward an enhanced metal function, to provide the beneficial effect on the hexadecane hydrocracking selectivity, preventing the excessive secondary cracking reactions [28].

In the present work, three industrially hierarchical Y zeolite samples with enhanced BET, as well as the elevated external surface area, as a result of the created meso- or/and macroporous structures due to the modification treatment, were prepared by industrially modifying an original USY zeolite sample. The introduced hierarchical porous system is conducive to the improved diffusion of the guest molecules in the zeolite crystals. Furthermore, the modification treatment on the Y zeolite has boosted the acid amount, especially the number of strong acid sites. The improved acid properties are attributed to the enhanced cracking role of the bifunctional catalysts, which were prepared by kneading the Y zeolite, alumina, nickel nitrate, and molybdenum oxide. The as-made bifunctional catalysts which utilized the hierarchical Y zeolites as the cracking components have displayed an excellent hydrocracking property suitable for light diesel oil, which meets the market needs.

2. Results and Discussion

2.1. Properties of the Industrial Y Zeolites

First, XRD patterns of the three samples, namely MUSY-A, -B, and -C, exhibited the typical characteristic diffraction peaks of faujasite structure, and no other impure peaks (not belonging to FAU zeolite) could be detected (Supplementary Materials Figure S1). The three industrial zeolites all have good crystallinity, in which MUSY-B and -C have somehow lower main diffraction peaks, as compared with MUSY-A.

The N₂ adsorption–desorption isotherms of MUSY-A, MUSY-B, and MUSY-C zeolite samples are illustrated in Figure 1. The adsorption–desorption of nitrogen on the MUSY-A sample is a combination of *type-I* and *type-IV* isotherms, mainly indicating the presence of micropores and aggregation of zeolite crystals (the loop). However, larger hysteresis loops occur in the adsorption–desorption isotherms of the MUSY-B and -C samples, indicating the presence of mesopores in the samples. The N₂ adsorption–desorption isotherms of MUSY-B and -C samples in Figure 1 display remarkable hysteresis loops after $p/p_0 = 0.45$, which can be caused by the secondary mesopores [10,15]. For MUSY-C, the sudden increase in N₂ adsorption after $p/p_0 \approx 0.8$, can be ascribed to the capillary condensation in open mesopores or macropores obtained [10,15,18]. In fact, the pore size distribution derived from the adsorption branch of the isotherms shows the existence of a meso- and macropore structure with a broad pore size distribution ranging from 3 to 50 nm in the zeolite samples (Supplementary Materials Figure S2). MUSY-B and -C have a very similar pore distribution, both with a narrow pore distribution, from 3 to 8 nm. Meanwhile, MUSY-A shows a larger amount of secondary meso- and macropores (10–50 nm) formed by ammonium hexafluorosilicate dealumination of parent zeolite Y.

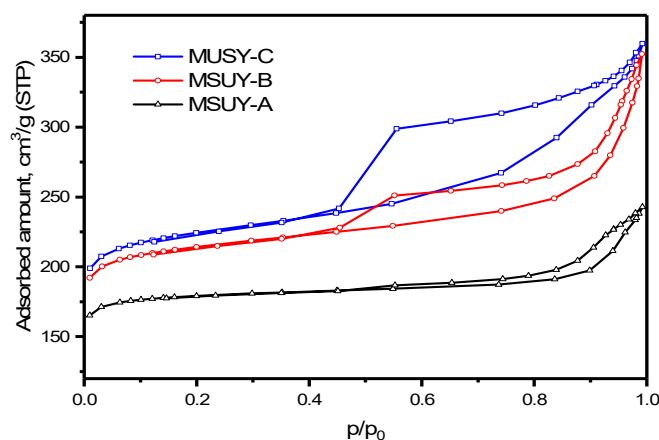


Figure 1. N₂ adsorption–desorption isotherms of the zeolites.

Second, SEM images of the used zeolite samples in Figure 2 suggest that the three zeolite crystals of MUSY-A, -B, and -C have basically the typical faujasite morphology with coarse external surface [14], while the external surfaces of the crystals in the latter two samples are coarser than those of the MUSY-A sample. In particular, the external surface of the sample MUSY-C is rather coarse in that many obvious nano-sized particles can be seen in the outer surface of its crystals. The TEM images of MUSY-B and -C (Figure 3) suggested strongly that abundant meso- and macropores appear in the two zeolite samples. The image of MUSY-A is compact and solid, indicating the presence of micropores and closed mesopores, which is in good agreement with the observed result by N₂ adsorption–desorption isotherms, as shown in Figure 1. Therefore, the steep increase after $p/p_0 = 0.8$ in the N₂ adsorption–desorption isotherm of MUSY-C can be ascribed to the capillary condensation in open mesopores or macropores obtained by filling the nano-sized Y zeolite interparticles' spaces in polycrystalline-like aggregations. In fact, direct evidence to illustrate the presence of intracrystalline mesopores or macropores with a size of ca. 20–80 nm in diameter is also provided by the TEM images.

The total pore volumes V_{total} of MUSY-A, -B, and -C zeolite samples are 0.36, 0.51, and 0.54 cm^3/g (Table 1), respectively, indicating the formation of more mesopores inside the crystals of the Y zeolite samples [29].

Table 1. Textural parameters and acid properties of the zeolite samples.

Samples	Surface Area (m^2/g)			Pore Volume (cm^3/g)			$\text{SiO}_2/\text{Al}_2\text{O}_3$	Brønsted	Lewis	B + L
	S_{BET}	S_{mic}	S_{ext}	V_{total}	V_{mic}	V_{meso}				
MUSY-A	690	624	66	0.36	0.25	0.12	9.8	0.49	0.08	0.57
MUSY-B	816	691	125	0.51	0.28	0.23	10.5	0.78	0.13	0.91
MUSY-C	852	702	150	0.54	0.28	0.26	10.4	0.90	0.16	1.06

S_{mic} t-plot micropore surface area; S_{ext} t-plot external surface area; V_{mic} t-plot micropore volume; V_{meso} BJH(Barret-Joyner-Halenda) mesopore volume ($V_{\text{total}} - V_{\text{micro}}$); $\text{SiO}_2/\text{Al}_2\text{O}_3$ mole ratio measured by XRF; B + L acid amount (mmol/g) of Brønsted and Lewis sites.

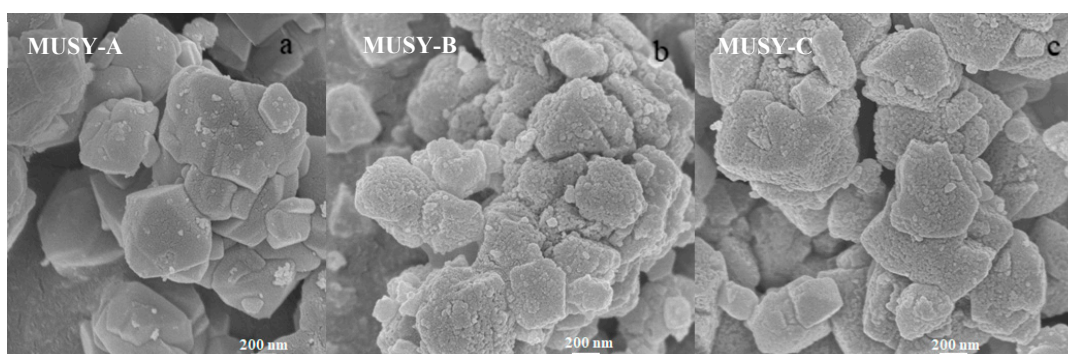


Figure 2. SEM images of the zeolites. MUSY-A (a), MUSY-B (b), and MUSY-C (c).

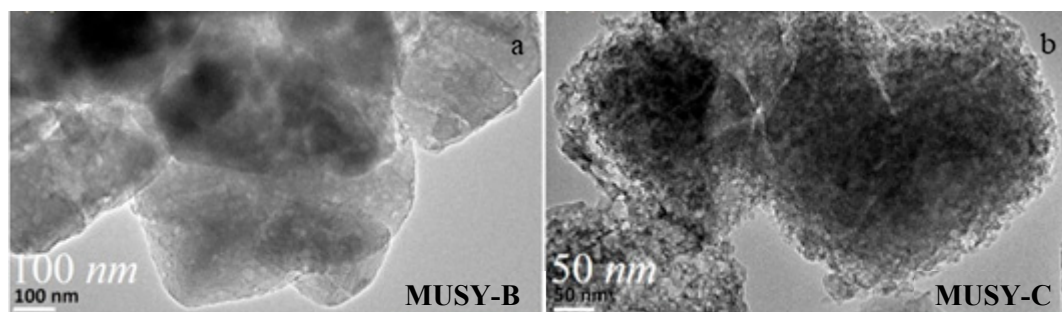


Figure 3. TEM images of the zeolites. MUSY-B (a) and MUSY-C (b).

In Figure 4, MAS NMR spectra of the MUSY-A, -B, and -C zeolite samples are presented. A keen-edged peak centering at about 57 ppm in ^{27}Al NMR spectra displayed at the lower right corner in Figure 4 is assigned to the tetrahedrally coordinated Al in the zeolite framework [18]. The peak at 0 ppm which is ascribed to octahedral coordinated Al atom is not observed in MUSY-B and -C samples. Meanwhile, an obvious peak centering at about 0 ppm, which is caused by non-framework aluminum, is detected in the sample MUSY-A, and a faint signal at 30 ppm assigned to the distorted tetrahedral or five-coordinated Al species [24] is also seen (see Supplementary Materials Figure S3). The result suggests that the framework and non-framework aluminum species coexist in the MUSY-A sample. However, the non-framework aluminum species disappeared after aluminizing (recrystallization) the parent MUSY-A (^{27}Al -NMR in Figure 4). Moreover, the signal centering at ca. 40–70 ppm in MUSY-B and -C is obviously narrower than that for MUSY-A zeolite, in which the widened peak may reflect the deterioration in the homogeneity of its framework aluminum atoms. For the ^{29}Si NMR spectra of all the three samples, the resonances around -110 ppm could be assigned to the Si

(4Si, 0Al) sites, those at -104 ppm to the Si(3Si, 1Al) sites, those at -98 ppm to the Si(2Si, 2Al) sites, and those at -93 ppm to the Si(1Si, 3Al) sites. The peak at -113 ppm is assigned to an amorphous silica phase [13]. The calculated framework Si/Al ratios of MUSY-A, MUSY-B, and MUSY-C are 10.9, 4.7, and 4.6, respectively. The framework Si/Al ratios calculated by the results obtained by ^{29}Si NMR spectra of the latter Y zeolite samples (MUSY-B and -C) are very similar to surface Si/Al ratios, as detected by XRF (Table 1), while the framework Si/Al ratio of MUSY-A is remarkably higher than the bulk Si/Al ratio (Table 1), manifesting a rich Al-species surface with non-framework aluminum (Figure 4 and Supplementary Materials Figure S3).

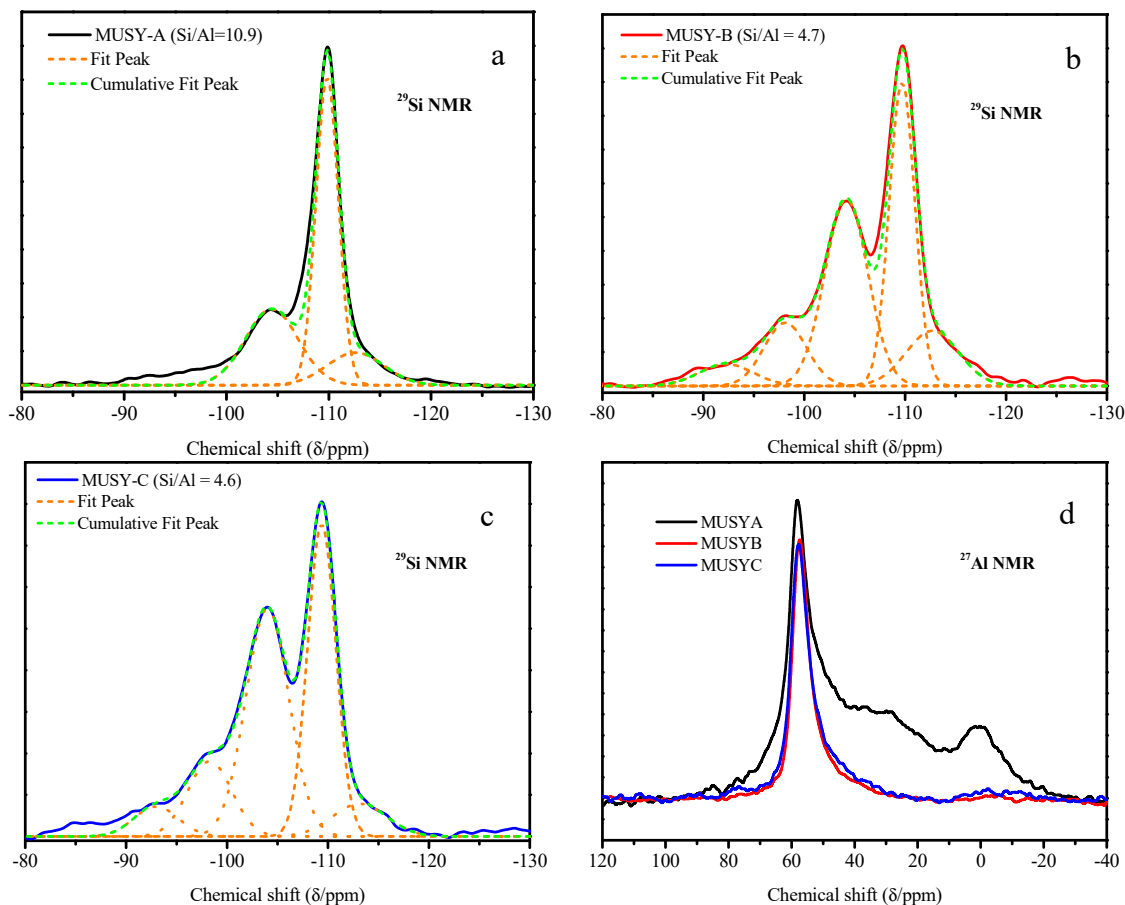


Figure 4. MAS NMR spectra of the zeolite samples. ^{29}Si NMR spectra of MUSY-A (a), -B (b) and -C (c), ^{27}Al NMR spectra of the three samples (d).

Consequently, the acid properties of the zeolite samples have been investigated by NH_3 -TPD (Figure 5) and in situ pyridine adsorption (Table 1). The NH_3 desorption peaks center at $217\text{--}233$ °C and $319\text{--}360$ °C and are ascribed to NH_3 escape from weak and/or strong acid sites, respectively [13,15]. The acid amounts obtained by calculating the corresponding peak areas of the NH_3 -TPD curves suggest that MUSY-B and -C have stronger acid intensity and more acid amounts than MUSY-A has. Based on the results of ^{29}Si NMR spectra of the three samples, the framework Si/Al ratio of MUSY-A is up to 10.9, and that of MUSY-B and of MUSY-C are 4.7 and 4.6, respectively. However, Si/Al ratios of the three samples by XRF method (Table 1) are very similar. Obviously, the MUSY-A sample, with higher framework Si/Al ratio, has more non-framework Al-species with the distorted tetrahedral or five-coordinated Al species (at 30 ppm; see Supplementary Materials Figure S3), to show a lower acid amount. The desorption peaks of NH_3 molecules centering at about 350 °C, which is attributed to the medium strong acid sites, has shifted from 339 °C in the curve of MUSY-A to 360 °C in that of MUSY-B and that of MUSY-C, indicating the existence of relatively stronger acid sites in them. MUSY-B

and MUSY-C display a good quantity of Brønsted acid amounts, Lewis acid amounts, and total acid amounts (Table 1), whose amount is much more than that of MUSY-A, which agrees fairly well with the results obtained by NH₃-TPD (Figure 5). The enhanced acid properties indicated by acid amount and strength in the two samples may give the corresponding catalysts excellent cracking properties.

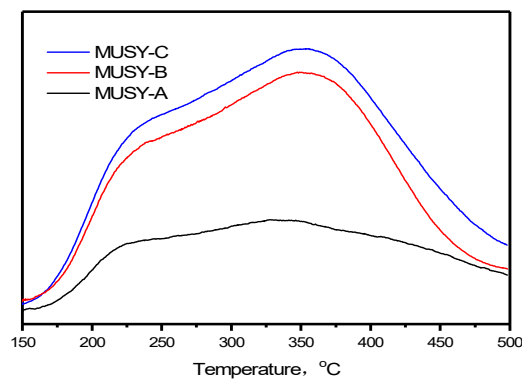


Figure 5. NH₃-TPD properties of the zeolite samples.

2.2. Hydrocracking Properties

The components of the light diesel oil, used in this experiment to serve as the feedstock, were determined by using the analysis method SH/T0606-2005 with gas chromatography/mass spectrometry (Waters 2695, American PerkinElmer Co., Waltham, MA, US). As shown in Table 2, diaromatics in the light diesel oil, including naphthalene, naphthalenes, acenaphthenes, and acenaphthylenes, reach up to 29.8 wt.%. Monoaromatics (mainly consisting of alkyl benzenes, indene) and tetrahydronaphthalene are 32.8 wt.%, cycloparaffins are 9.1 wt.%, and others, mainly paraffins, are 28.2 wt.%. A blank measurement over the catalyst without zeolite has indicated the hydrogenation function in the process, in which cycloparaffins and alkyl benzenes components increase obviously, while diaromatics decrease markedly.

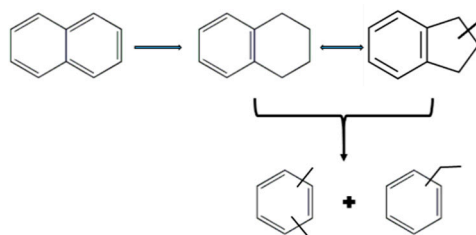
Table 2. Hydrocracking product distributions (wt.%) over the catalysts HCK-A, -B, and -C.

Components	Feedstock	Blank	HCK-A	HCK-B	HCK-C	Error (%)
Paraffins	28.2	23.6	29.2	28.8	29.1	±1.5
Cycloparaffins	9.3	17.8	10.0	10.3	10.1	±2.0
Alkyl benzenes	20.4	26.9	24.7	25.4	27.5	±1.0
Indene or tetralin	12.2	18.5	30.8	29.4	27.2	±1.0
Diaromatics	29.9	11.2	5.2	6.1	7.1	±1.5

Reaction conditions: hydrogen partial pressure, 4.0 MPa; LHSV, 2 h⁻¹; hydrogen/oil (v/v), 600; temperature, 320 °C.

The catalytic hydrocracking performance of the light diesel oil was evaluated on a microreactor unit. The results in Table 2 (and Supplementary Materials Figure S4) show distinctions in the light diesel oil product distribution for the three catalysts, indicating their different catalytic properties, respectively. After being treated by the hydrocracking catalysts, the diaromatics in the light diesel oil decreased remarkably, from 29.8 to 5.2~7.1 wt.%, while the hydrogenation products, for example, the indene and tetrahydronaphthalene, increased from 3.1 to about 27.2~30.8 wt.%, and the alkyl benzenes increased from 20.4 to 24.7~27.5 wt.%. The aforementioned results suggest that all the bifunctional catalysts display excellent hydrogenation and ring-opening (cracking) activity.

Hydrogenation–dehydrogenation function afforded by Mo and Ni metals transforms diaromatics into indene or tetralin, which can then be transformed into alkyl benzenes when subjected to cracking or ring-opening processing over the acid sites, mainly in the zeolite. It can be suggested from Table 2 that the catalysts using MUSY-B and -C as the cracking active component display less selectivity for indene and tetralin but better selectivity for alkyl benzene, indicating that MUSY-B and -C have higher cracking activity as compared with MUSY-A because of the improved acid properties and the elevated diffusion efficiency, as a result of the secondary meso- and macropore structures created. The zeolite samples MUSY-B and -C have very similar properties; the catalyst HCK-C has stronger ring-opening ability than HCK-B, resulting from its high yield of alkylbenzenes and low selectivity of indans/tetralins in the products (Table 1 and Supplementary Materials Figure S4) because of more Brønsted acid sites in MUSY-C (Table 1). It is well-known that the hydrocracking performances of the catalysts are strongly determined by the acidity and the acid sites' accessibility of zeolite component, and Brønsted acidity afforded by the zeolite component plays a key role in the acid-catalyzed reactions during hydrocracking [30]. The accessible Brønsted acid sites contributing to the cracking performances usually depend on textural properties of the zeolite component. The diffusion limitations of the micropores with similar window-sizes in the zeolites to the reactant molecules not only decrease the reaction activity because of the limited accessibility of the active sites located mostly in the micropores and microchannels, but also may give deteriorated selectivity due to secondary cracking of the products [31]. Anyway, the introduced meso- or/and macropore structure into the zeolite component is beneficial for hydrocracking [30,32] by alleviating the diffusion limitation due to the shortened micropores, or facilitating the transport of bulky hydrocarbon molecules with the existence of the larger pores. The aforementioned results detected by NH₃-TPD and in situ pyridine adsorption showed that the modification treatment has given the MUSY-B and MUSY-C more acidity (especially more Brønsted acid sites; see Table 1) and stronger acid strength. The more Brønsted acid sites mean more active sites which can be utilized by the reactants, while the stronger acidity attributes to the elevated cracking roles of the reactants. Moreover, the created hierarchical pores represented by the meso- and macroporous system, as detected by N₂ adsorption–desorption experiments and verified by TEM images, have improved the accessibility of the acid sites for the bulky reactants [9,16,17,30], especially for the bulky reactant molecules [24], for example, the indene and tetralin. The increased diffusion efficiency is also conducive to the depressed overcracking [31], which further contributes to the higher selectivity toward alkyl benzenes. A scheme of hydrocracking of naphthalene over the catalysts is suggested, as follows (Scheme 1):



Scheme 1. Hydrocracking of naphthalene over the catalysts.

Finally, the catalysts were further investigated during the hydrocracking of the same light diesel oil under different temperatures, to evaluate the effect of temperature on the hydrocracking efficiency (Figure 6). Obviously, the yield of alkyl benzenes increased with the temperature increasing at 240–300 °C, while it decreased with the temperature increasing above 320 °C. When the temperature exceeds 320 °C, the high temperature could easily lead to secondary cracking [31], which makes the alkyl benzene yield decrease.

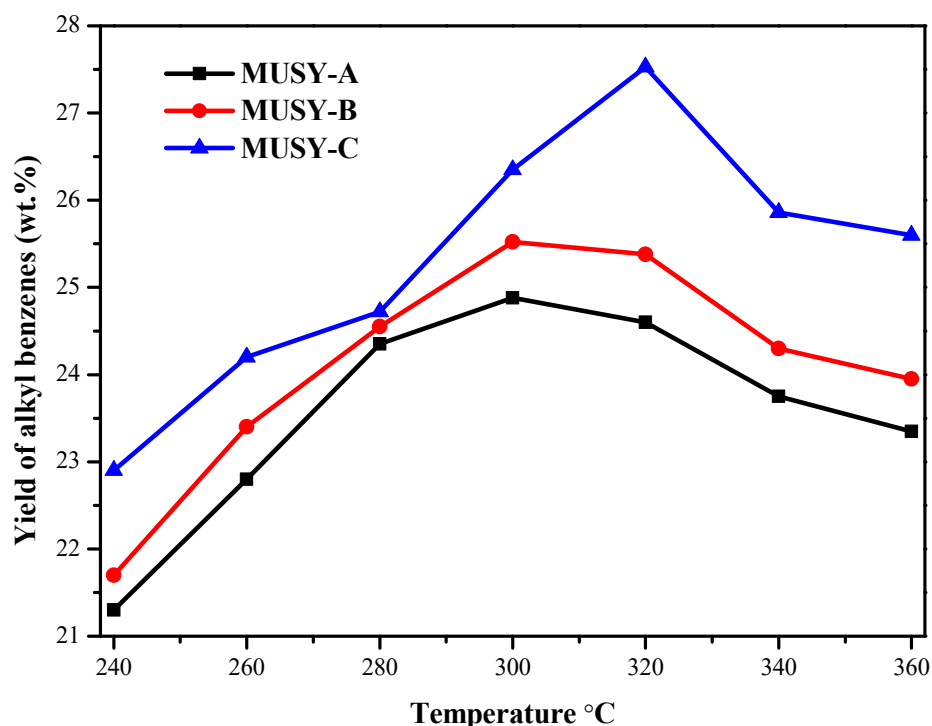


Figure 6. Effect of temperature on the yield of alkylbenzenes in the hydrocracking products over the catalysts containing MUSY-A, MUSY-B, and MUSY-C.

3. Materials and Methods

3.1. Preparation of Hydrocracking Catalysts

The three industrial Y zeolites selected, named MUSY-A, MUSY-B, and MUSY-C in the work, were from the Dalian Research Institute of Petroleum and Petrochemicals. MUSY-A is a commercial industrial product USY zeolite produced by Dalian (Fushun) Research Institute of Petroleum & Petrochemicals, SINOPEC. The preparation conditions were pre-optimized in order to obtain the required samples industrially. MUSY-B and MUSY-C are the modified USY zeolite samples by recrystallizing the parent MUSY-A sample in ca. 0.15 and 0.45 mol L⁻¹ NaOH solutions with a special template (non-ionic surfactant, fatty alcohol-polyoxyethylene ether) at 90 and 100 °C (aluminizing), respectively. The solid/liquid ratios (zeolite/NaOH aqueous solution) were 5–10 g/mL. The textural parameters of these Y zeolites (the contents of sodium oxide are below 1.0 wt.%) are listed in Table 1. The hydrocracking catalyst was prepared by homogeneously kneading the industrial Y zeolite (10 wt.%), commercial alumina (supplied from Dalian Research Institute of Petroleum and Petrochemicals, Fushun/Dalian, China, 68 wt.%), nickel nitrate (Beijing Chemical Co., Beijing, China, 5.0 wt.%), and molybdenum oxide (Beijing Chemical Co., 17.0 wt.%), and then extruding the mixture to get strip extrudate, which was dried at 120 °C for 5 h in air, followed by calcination at 500 °C for 3 h in a muffle furnace. The particles of metal oxide dispersed uniformly on the surface of alumina, which are consistent with those reported in the literature [30]. The three bifunctional catalysts prepared by using MUSY-A, MUSY-B, and MUSY-C were labeled HCK-A, HCK-B, and HCK-C, respectively. The preparation reference catalyst (black sample in Table 2) followed exactly the same process as the former, with only silica instead of zeolite.

3.2. Characterization Methods

X-ray powder diffraction (XRD) was carried out by using a D/MAX-2500 X-ray diffractometer (Rigaku Corporation, Tokyo, Japan) with Cu K α radiation in the 2 θ angle range of 5–40° and at a scanning rate of 8 °/min. The incident wavelength was 0.15405 nm, the tube current was 80 mA, and the voltage was 40 kV.

N₂ adsorption–desorption isotherm was measured by using an ASAP 2420 Micromeritics instrument at the liquid-nitrogen temperature. The Brunauer–Emmett–Teller (BET) equation was used to calculate the total specific surface area. The microporous and external surface area were calculated by the t-pot method. Pore size distributions were obtained by using the BJH model.

Scanning electron microscopy (SEM) images were obtained on a JEOL 7500F SEM with accelerating voltage at 0.1–30 kV. Transmission electron microscopy (TEM) was performed on a JEM 2100 electron microscope with voltage at 200 kV.

Surface acid sites (Brønsted and Lewis) of the zeolites were characterized by IR spectroscopy of adsorbed pyridine. IR spectra were recorded on a Shimadzu IR Affinity-1 spectrometer (Tokyo, Japan). All samples were pressed in self-supporting wafers and activated in a vacuum IR cell at 500 °C for 4 h prior to the adsorption of probe molecules. Pyridine was introduced at room temperature. The numbers of acid sites were calculated from the integrated area and intensity of given bands with the distinct molar extinction coefficients.

Solid-state NMR spectra were recorded on a Bruker Avance III 500 spectrometer (Karlsruhe, Germany), at the resonance frequencies of 99.4 and 130.3 MHz; 5 and 8 kHz sample spinning rates; 0.22 and 0.9 μ s pulse widths; 4 and 1 s recycle delays; and 1024 and 1000 sampling frequencies for ²⁹Si-NMR and ²⁷Al-NMR, respectively. The sample packing system provided 7.0 and 4.0 mm rotors for ²⁹Si-NMR and for ²⁷Al-NMR, respectively. The following formula was used to calculate the overall Si/Al ratio of the framework:

$$\frac{\text{Si}}{\text{Al}} = \frac{\sum_{n=0}^4 I_n}{\sum_{n=0}^4 \frac{4}{n} I_n}$$

where I_n is the intensity of the peak associated with Q₄ (nAl).

The acidity of the samples was measured by NH₃ temperature programmed desorption (NH₃-TPD), using Micromeritics Autochem 2910 instrument. In typical a process of NH₃-TPD analysis, 100 mg zeolite was placed in a container and heated to 600 °C, with heating rate of 8 °C/min, in He flow for 1 h. Then it was cooled to 120 °C in He flow, and at this condition, 0.15% NH₃ was transited to the zeolite for 1 h. NH₃ desorption was investigated from 150 to 500 °C, with the heating rate of 8 °C/min in He flow.

3.3. Catalyst Evaluation

Hydrocracking of light diesel oil was carried out in a fixed-bed stainless-steel tubular reaction system, with the feedstock oil introduced into the reactor through a syringe pump. The feedstock consisted of pretreated Maoming light diesel oil. Then, 5 mL of the catalysts (20~40 mesh size) was diluted with 5 mL inert sand (~30 mesh size). Prior to the reaction, the system was pressurized to 4 MPa with hydrogen and H₂ flow rate of 100 mL/min, and the catalysts were sulfided with a mixture of sulfide oil (2 wt.% of carbon disulfide and 98 wt.% of n-dodecane) at 230 °C for 4 h. The particle size of the sulfided metal oxide was ca. 10 nm. A liquid hourly space velocity (LHSV) of 2 h⁻¹ was set and maintained before the light diesel oil injection. Hydrocracking tests were carried out at 240~360 °C. The average deactivation rate of the catalyst in industry was 1.2 \times 10⁻² °C/day, and also the catalyst has excellent regeneration property. The catalyst which had operated in industry for three years was regenerated, so the catalytic property recovered to 95% of the fresh catalyst.

4. Conclusions

Three industrially hierarchical Y zeolites were used to prepare the hydrocracking catalyst of light diesel oil. The bifunctional hydrocracking catalysts were obtained by kneading the Y zeolite sample, commercial alumina, nickel nitrate, and molybdenum oxide, and later by the extruding process. The presence of mesopores in the Y zeolites has improved the accessibility of the acid sites for the bulky reactants. The catalytic results over the catalysts include the decrease of diaromatics and the increase of mono-aromatics and -cyclanes in the products. The increase in the yield of alky benzenes is owed to the ring-opening reaction by cracking on the acid sites of the Y zeolites following hydrogenation on metals. With only 10 wt.% the zeolite in the hydrocracking catalyst, the hierarchical pore structures and the increased Brønsted acid sites improved their acidity and enhanced the accessibility of the bulky molecule reactants. In the future, discovering how to increase the ring-opening ability of the Y zeolites to indene and/or tetralin to produce BTX will be challenging work.

Supplementary Materials: The following are available online at <http://www.mdpi.com/2073-4344/10/8/815/s1>, Figure S1: XRD patterns of the zeolite samples, Figure S2: BJH pore size distribution of the adsorption branch of zeolites, Figure S3: TEM images of the zeolites. MUSY-B and MUSY-C (Right), Figure S4: ^{27}Al MAS NMR Spectra of the samples, Figure S5: NH_3 -TPD properties of the zeolite samples, Figure S6: Hydrocracking products distributions over the catalysts containing MUSY-A, MUSY-B and MUSY-C.

Author Contributions: J.M. conceived and designed the experiments; B.Q. and M.Z. performed the experiments; R.L. and J.Z. analyzed the data; B.Q. and Y.D. contributed the catalyst preparation and industrial catalytic tests; M.Z. and W.Z. completed characterization; J.M. and M.Z. wrote the paper; R.L. revised and edited the paper. All authors have read and agreed to the published version of the manuscript.

Funding: The research was funded by NSFC (U19B2003, 21371129) and SinoPEC (119010-1).

Acknowledgments: The work was supported by Shanxi Province Key Innovative Research Team in Science and Technology (No.2014131006). We honestly thank Tao Hou for her help in technology English.

Conflicts of Interest: The authors declare no conflict of interest.

References

1. Manrique, C.; Guzman, A.; Pérez, P.J.; Márquez, A.C.; Echavarría, A. Effect of synthesis conditions on zeolite Beta properties and its performance in vacuum gas oil hydrocracking activity. *Microporous Mesoporous Mater.* **2016**, *234*, 347–360. [[CrossRef](#)]
2. Hassan, A.; Ahmed, S.; Ali, M.A.; Hamid, H.; Inui, T. A comparison between β - and USY-zeolite-based hydrocracking catalysts. *Appl. Catal. A* **2001**, *220*, 59–68. [[CrossRef](#)]
3. Gutiérrez, A.; Arandes, J.M.; Castaño, P.; Olazar, M.; Barona, A.; Bilbao, J. Effect of space velocity on the hydrocracking of Light Cycle Oil over a Pt-Pd/HY zeolite catalyst. *Fuel Process. Technol.* **2012**, *95*, 8–15.
4. Ding, L.; Zheng, Y.; Zhang, Z.; Ring, Z.; Chen, J. HDS, HDN, HAD, and hydrocracking of model compounds over Mo-Ni catalysts with various acidities. *Appl. Catal. A* **2007**, *319*, 25–37. [[CrossRef](#)]
5. Ishihara, A.; Itoh, T.; Nasu, H.; Hashimoto, T.; Doi, T. Hydrocracking of 1-methylnphthalene/decahydronaphthalene mixture catalyzed by zeolite-alumina composite supported NiMo catalysts. *Fuel Process. Technol.* **2013**, *116*, 222–227. [[CrossRef](#)]
6. Seo, M.; Lee, D.; Lee, K.Y.; Moon, D.J. Pt/Al-SBA-15 catalysts for hydrocracking of C21-C34 n-paraffin mixture into gasoline and diesel fractions. *Fuel* **2015**, *143*, 63–71. [[CrossRef](#)]
7. Tailleux, R.G.; Nascar, J.R. The effect of aromatics on paraffin mild hydrocracking reactions (W_{Ni}Pd/CeY-Al₂O₃). *Fuel Process. Technol.* **2008**, *89*, 808–818. [[CrossRef](#)]
8. Alsobaai, A.M.; Zakaria, R.; Hameed, B.H. Characterization and hydrocracking of gas oil sulfide NiW/MCM-48 catalysts. *Chem. Eng. J.* **2007**, *132*, 173–181. [[CrossRef](#)]
9. Sato, K.; Nishimura, Y.; Honna, K.; Matsubayashi, N.; Shimada, H. Role of HY zeolite mesopores in hydrocracking of heavy oils. *J. Catal.* **2001**, *200*, 288–297. [[CrossRef](#)]
10. Zhao, Q.; Qin, B.; Zheng, J.; Du, Y.; Sun, W.; Ling, F.; Zhang, X.; Li, R. Core-shell structured zeolite-zeolite composites comprising Y zeolite cores and nano- β zeolite shells: Synthesis and application in hydrocracking of VGO oil. *Chem. Eng. J.* **2014**, *257*, 262–272. [[CrossRef](#)]

11. Al-Khattaf, S.; Tukur, N.M.; Al-Amer, A.; Al-Mubaiyeth, U.A. Catalytic transformation of C7–C9 methyl benzenes over USY-based FCC zeolite catalyst. *Appl. Catal. A* **2006**, *305*, 21–31. [[CrossRef](#)]
12. Ishihara, A.; Fukui, N.; Nasu, H.; Hashimoto, T. Hydrocracking of soybean oil using zeolite-alumina composite supported NiMo catalysts. *Fuel* **2014**, *134*, 611–617. [[CrossRef](#)]
13. Aelst, J.V.; Haouas, M.; Gobechiya, E.; Houthoofd, K.; Philippaerts, A.; Sree, S.P.; Kirschhock, C.E.A.; Jacobs, P.; Martens, J.A.; Sels, B.F.; et al. Hierarchization of USY zeolite by NH₄OH. A postsynthetic process investigated by NMR and XRD. *J. Phys. Chem. C* **2014**, *118*, 22573–22582. [[CrossRef](#)]
14. Doyle, A.M.; Albayati, T.M.; Abbas, A.S.; Alismael, Z.T. Biodiesel production by esterification of oleic acid over zeolite Y prepared from kaolin. *Renew. Energy* **2016**, *97*, 19–23. [[CrossRef](#)]
15. Zhao, J.; Wang, G.; Qin, L.; Li, H.; Chen, Y.; Liu, B. Synthesis and catalytic cracking performance of mesoporous zeolite Y. *Catal. Commun.* **2016**, *73*, 98–102. [[CrossRef](#)]
16. Hosseinpour, N.; Mortazavi, Y.; Bazyari, A.; Khodadadi, A.A. Synergetic effects of Y-zeolite and amorphous silica-alumina as main FCC catalyst components on tripropylbenzene cracking and coke formation. *Fuel Process. Technol.* **2009**, *90*, 171–179. [[CrossRef](#)]
17. Li, W.; Zheng, J.; Luo, Y.; Da, Z. Effect of hierarchical porosity and phosphorus modification on the catalytic properties of zeolite Y. *J. Appl. Surf. Sci.* **2016**, *382*, 302–308. [[CrossRef](#)]
18. Martínez, J.G.; Johnson, M.; Valla, J.; Li, K.; Ying, J.Y. Mesostructured zeolite Y-high hydrothermal stability and superior FCC catalytic performance. *Catal. Sci. Technol.* **2012**, *2*, 987–994. [[CrossRef](#)]
19. Agudelo, J.L.; Mezari, B.; Hensen, E.M.; Giraldo, S.A.; Hoyos, L.J. On the effect of EDTA treatment on the acidic properties of USY zeolite and its performance in vacuum gas oil hydrocracking. *Appl. Catal. A* **2014**, *488*, 219–230. [[CrossRef](#)]
20. Sachse, A.; Wuttke, C.; Díaz, U.; Souza, M.O. Mesoporous Y zeolite through ionic liquid based surfactant templating. *Microporous Mesoporous Mater.* **2015**, *217*, 81–86. [[CrossRef](#)]
21. Zhao, Y.; Liu, Z.; Li, W.; Zhao, Y.; Pan, H.; Liu, Y.; Li, M.; Kong, L.; He, M. Synthesis, characterization, and catalytic performance of high-silica Y zeolites with different crystallite size. *Microporous Mesoporous Mater.* **2013**, *167*, 102–108. [[CrossRef](#)]
22. Chang, X.W.; He, L.F.; Liang, H.N.; Liu, X.; Yan, Z. Screening of optimum condition for combined modification of ultra-stable Y zeolites using multi-hydroxyl carboxylic acid and phosphate. *Catal. Today* **2010**, *158*, 198–204. [[CrossRef](#)]
23. García, J.R.; Bertero, M.; Falco, M.; Sedran, U. Catalytic cracking of bio-oils improved by the formation of mesopores by means of Y zeolite desilication. *Appl. Catal. A* **2015**, *503*, 1–8. [[CrossRef](#)]
24. Agudelo, J.L.; Hensen, E.J.M.; Giraldo, S.A.; Hoyos, L.J. Influence of steam-calcination and acid leaching treatment on the VGO hydrocracking performance of faujasite zeolite. *Fuel Process. Technol.* **2015**, *133*, 89–96. [[CrossRef](#)]
25. Yan, Z.; Ma, D.; Zhuang, J.; Liu, X.; Liu, X.; Han, X.; Bao, X.; Chang, F.; Xu, L.; Liu, Z. On the acid-dealumination of USY zeolite: A solid state NMR investigation. *J. Mol. Catal. A: Chem.* **2003**, *194*, 153–167. [[CrossRef](#)]
26. Zhang, P.; Wang, X.; Guo, X.; Guo, H.; Zhao, L.; Hu, Y. Characterization of modified nanoscale ZSM-5 zeolite and its application in the olefins reduction in FCC gasoline. *Top. Catal.* **2004**, *92*, 63–68.
27. Kazakov, M.O.; Nadeina, K.A.; Danilova, I.G.; Dik, P.P.; Klimov, O.V.; Pereyma, V.Y.; Paukshtis, E.A.; Golubev, I.S.; Prosvirin, I.P.; Gerasimov, E.Y.; et al. Influence of USY zeolite recrystallization on physicochemical properties and catalytic performance of NiMo/USY-Al₂O₃ hydrocracking catalysts. *Catal. Today* **2019**, *329*, 108–115. [[CrossRef](#)]
28. Bukhtiyarova, M.V.; Toktarev, A.V.; Kazakov, M.O.; Kodenev, E.G.; Pereyma, V.Y.; Gabrienko, A.A.; Bukhtiyarov, A.V.; Echevsky, G.V. Effect of sulfosalicylic acid treatment on the properties of Beta zeolite and performance of NiW/Beta-based catalysts in hexadecane hydrocracking. *Appl. Catal. A* **2020**, *598*, 117573. [[CrossRef](#)]
29. Benazzi, E.; Leite, L.; Marchal-George, N.; Toulhoat, H.; Raybaud, P. New insights into parameters controlling the selectivity in hydrocracking reactions. *J. Catal.* **2003**, *217*, 376–387. [[CrossRef](#)]
30. Kazakov, M.O.; Nadeina, K.A.; Danilova, I.G.; Dik, P.P.; Klimov, O.V.; Pereyma, V.Y.; Gerasimov, E.Y.; Dobryakova, I.V.; Knyazeva, E.E.; Ivanova, I.I.; et al. Hydrocracking of vacuum gas oil over NiMo/Y-Al₂O₃: Effect of mesoporosity introduced by zeolite Y recrystallization. *Catal. Today* **2018**, *305*, 117–125. [[CrossRef](#)]

31. Landau, M.V.; Vradman, L.; Valtchev, V.; Lezervant, J.; Liubich, E.; Talianker, M. Hydrocracking of heavy vacuum gas oil with a Pt/H-beta-Al₂O₃ catalyst: Effect of zeolite crystal size in the nanoscale range. *Ind. Eng. Chem. Res.* **2003**, *42*, 2773–2782. [[CrossRef](#)]
32. De Jong, K.P.; Zečević, J.; Friedrich, H.; De Jongh, P.E.; Bulut, M.; Van Donk, S.; Kenmogne, R.; Finiels, A.; Hulea, V.; Fajula, F. Zeolite|Y crystals with trimodal porosity as ideal hydrocracking catalysts. *Angew. Chem.* **2010**, *122*, 10272–10276. [[CrossRef](#)]



© 2020 by the authors. Licensee MDPI, Basel, Switzerland. This article is an open access article distributed under the terms and conditions of the Creative Commons Attribution (CC BY) license (<http://creativecommons.org/licenses/by/4.0/>).